

Cluster ion emission in the interaction of slow highly charged ions with surfaces

T. Schenkel, A.V. Barnes, A.V. Hamza^a, and D.H. Schneider

University of California Lawrence Livermore National Laboratory Livermore, CA 94551, USA

Received: 22 April 1997 / Revised: 29 December 1997 / Accepted: 19 January 1998

Abstract. Cluster ion emission from a variety of surfaces upon impact of highly charged ions is investigated by time-of-flight secondary ion mass spectrometry. The yield of cluster ions as a function of cluster size for SiO₂ and C₈₄ surface follow a power law decline with exponent approaching the -2 limit of the “equilibrium” and “shock wave” cluster emission models. While the decline of the cluster ion emission with cluster size is an exponential decay for highly oriented pyrolytic graphite upon Th⁷⁰⁺ impact, the decline is more gradual than for Cs¹⁺ impact, such that at C₁₆ the relative cluster yield is 1000 times higher.

PACS. 36.40.c Atomic and molecular clusters – 61.46.+w Clusters, nanoparticles, and nanocrystalline materials – 82.65.Yh Other surface and interface chemical processes

1 Introduction

Production of high yields of secondary cluster ions is one of the characteristic features of highly charged ion (HCI) inducing sputtering of materials [1–3]. The change in cluster intensities as a function of cluster size in sputtering of different materials has been used as a signature for the presence of distinct cluster production and sputtering mechanisms. One basic question is whether clusters are emitted from a surface as an intact entity, or rather form at the surface from independently excited atoms.

The most easily measured quantity is the mass distribution of ionized clusters. Post-ionization of neutral clusters may lead to their fragmentation which may render the interpretation of neutral mass distributions difficult. A difficulty with cluster ion yields is the dependency of ionization probability and electron affinities on cluster size. Wucher *et al.* [4] have shown via comparison of neutral cluster yields measured by laser post-ionization and ionized cluster yields that the ionization probability and electron affinity for clusters greater than $n = 5$ is fairly constant, though oscillation of ion stabilities are observed.

Measurements of cluster ion yields at short times (much less than $1 \mu\text{s}$) are do not exhibit oscillations [5]. Mass spectra at late time (greater than $1 \mu\text{s}$) are influenced by relative cluster ion stabilities [5]. Most clusters decay by evaporation of single neutral atoms [6].

In the measurements presented here the cluster ions are in the intermediate time regime of $\sim 1 \mu\text{s}$. As is shown below effects due to cluster ion stability are observed. However, the smoothed, intermediate-time cluster

ion distribution is representative of the early time distribution. Since ion production occurs at short times, cluster ion stability is unimportant in the ion production process. Thus, the distribution of ionized clusters for larger cluster, $n > 5$, gives a relatively faithful picture of the relative neutral cluster distribution.

The collision cascade model has been very successful in the description of monoatomic secondary ion emission in the interaction of keV, singly charged ions with surfaces [7]. Independent atom-atom collisions along a collision cascade result in the ejection of surface and near-surface atoms. Secondary particle yields increase proportional to the nuclear stopping power of the incident ions in a target material. In experimental studies, most of the secondary particles are found to be neutral, and significant contributions from molecular secondary particles (both charged and neutral) are observed. However, the linear cascade theory cannot explain the yields of clusters for singly charged projectiles [8,9].

In the “statistical molecule emission” picture [10], it is assumed that clusters form at the surface after constituting atoms have received kinetic energy in independent, random collisions from the same collision cascade. Clusters can form if the center-of-mass energy of the contributing atoms and molecules is smaller than the dissociation energy of the cluster. This combinatorial model predicts an exponential decay of secondary cluster yields with increasing cluster size [8].

In contrast to the combinatorial model, an “emission-as-entity” model predicts a power law dependence of the yields of emitted clusters with increasing cluster size. The assumption is that momentum is transferred to near-surface target molecules due to the propagation of a

^a e-mail: hamza1@llnl.gov

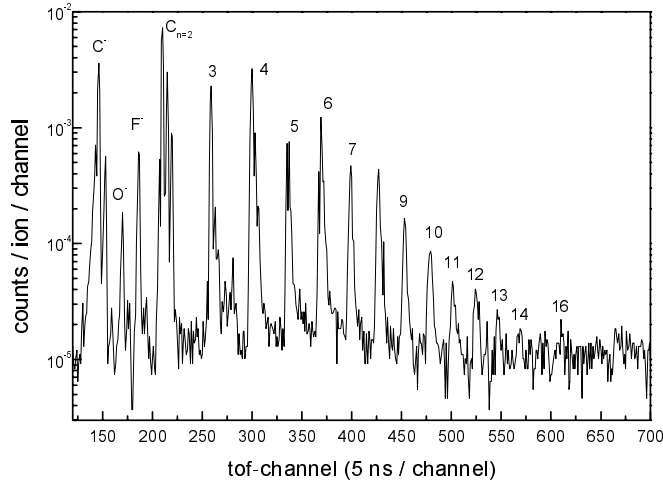


Fig. 1. Negative secondary ion production from HOPG at Th^{70+} impact. Incident kinetic energy is 3 keV/u and the total C_n^- counts/ion are 0.14.

pressure pulse or shock wave [11, 12], resulting in the emission of large clusters. The predicted exponent for the power law is ~ -2 [8, 12].

The cluster sputtering model by Urbassek [9] is applicable to sputtering by both singly and highly charged ions. In this “equilibrium” model, a highly energized region of the surface undergoes a liquid-gas phase transition upon expanding into vacuum. If the phase transition happens near the critical point (where interparticle binding is just balanced by the kinetic energy), fluctuations are high enough to produce high yields of large clusters. In this model the clusters are assumed to be in equilibrium with each other and monoatomic species. The cluster yield depends on the energy deposited into the near-surface volume, since to reach the critical point the kinetic energy of the target atoms have to be high, so that chemical bonding loses its importance and the system becomes fluid. Slow, highly charged ions can deposit a large amount of potential energy (100-300 keV per ion) into a small nanometer sized volume on very short, femtosecond, time scales [13, 14]. The equilibrium model predicts transitions from an exponential decay to power law decay as the phase transition occurs closer to the critical point. The dependence of the cluster yield $Y(n)$ on the cluster size, n , is

$$Y(n) = Y_0 n^{-\tau} \exp[(-\Delta G n - 4\pi n^{2/3} r^2 \sigma) / kT] \quad (1)$$

where ΔG is the difference of the Gibbs free energies of the liquid and gas phase, k is Boltzmann’s constant, T is the temperature of the energized region, Y_0 is the sputter yield (a constant for a given projectile-target system), r is the cluster radius, σ is the surface tension and τ is the critical exponent. At equilibrium ΔG is zero and at the critical point the surface tension vanishes. Thus, the power law exponent at the critical point is $-\tau$, with $-\tau$ between -2 and -2.5 . It follows that predicted cluster size distributions are very similar for the equilibrium and shock wave models.

In this paper the emission of clusters from surfaces upon impact of highly charged ions will be presented. The cluster ion yield *versus* cluster size will be discussed in the context of the above models. Studies of positive, atomic secondary ion production as a function of projectile charge have been presented in references [3, 14].

2 Experimental

Highly charged ions were extracted from the electron beam ion trap (EBIT) at Lawrence Livermore National Laboratory [15]. A bending magnet in the beamline between the EBIT and the UHV scattering chamber (base pressure $< 3 \times 10^{-8}$ Pa) is used to select the mass-to-charge ratio of the incident ion beam. Time-of-flight secondary ion mass spectrometry (TOF-SIMS) was performed to measure cluster yields. The system is described in references [1] and [3]. Briefly, fluxes of < 1000 ions per second were used and each TOF-SIMS cycle was triggered by secondary particles emitted from the target at impact of an individual HCI under normal incidence. High yields of electrons and protons were used as start pulses for the time-of-flight for negative and positive secondary ions, respectively. Start efficiencies were 100% for electron starts and between 10 and 80% for proton starts. Start signals and secondary ion stop signals were detected by the same annular microchannel plate detector. The microchannel plate detection efficiency for secondary ions is estimated from the solid angle subtended and the active area to be ~ 10 to 15%. TOF-SIMS spectra are recorded with a multi-stop multichannel scaler.

The following target samples were used. HOPG samples were cleaved in air just prior to being installed in vacuum. 150 nm thermal oxide on silicon wafers were cleaned by the “RCA” procedure and installed as received. The HOPG and SiO_2 samples were sputter cleaned (3 keV Xe^+ ions, 45 degree angle of incidence, 1–2 μA for 10–15 minutes) *in situ*. The SiO_2 surface was also annealed to 900 K after sputter cleaning. No difference in the relative cluster ion yields were seen in the annealed and unannealed cases. The oxygen yield was, however, higher from the annealed sample, suggesting the sputter cleaning slightly depletes the surface in oxygen, but not enough to affect the cluster ion yield. Micron thick C_{60} and C_{84} films were vacuum deposited on silicon (100) wafers; the native oxide was not removed before deposition. After deposition the cool sample was exposed to atmosphere in the transfer to the scattering chamber. No *in-situ* cleaning of the fullerene samples was performed since sputtering would damage the fullerene cages and annealing can produce polymerization of the clusters. Fullerene surfaces are fairly inert in air and can be used to protect surfaces due to their hydrophobicity [16, 17].

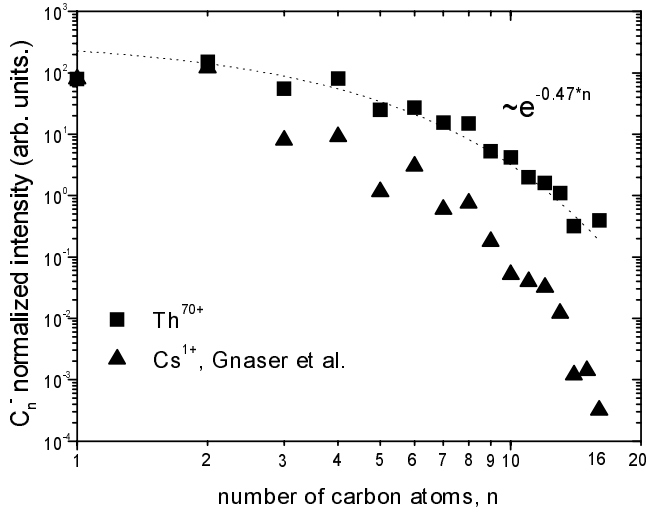


Fig. 2. Negative cluster ion intensities *versus* cluster size, n , for sputtering of HOPG by Th^{70+} (3KeV/u). Cs^{1+} (0.11 keV/u) sputtering of HOPG from reference [18].

3 Results and discussion

3.1 Highly oriented pyrolytic graphite

Using Th^{70+} ions ($E_{\text{kin}} = 3 \text{ keV/u}$) we have investigated negative secondary ion production from highly oriented pyrolytic graphite (HOPG) samples (see Fig. 1). Carbon clusters from C_1^- to C_{16}^- are observed with yields ranging from 10^{-2} to a couple times 10^{-5} counts per incident primary ion. The yield *versus* size dependency exhibits an odd-even oscillation, well known from singly charged ion-induced sputtering [18]. It has been found in UV photoelectron spectroscopy [7, 18] studies that carbon clusters with $n < 10$ have linear chain-like structures, while larger ones form monocyclic rings. Favoring odd or even numbered carbon clusters reflects changes in cluster electron affinities which are in turn sensitive to these different cluster geometries.

The striking difference between HCI and singly charged ion cluster sputtering is the rate of intensity change with increasing cluster size (see Fig. 2). The yield for cluster ions for the Th^{70+} case and the Cs^{1+} (14 keV) case [18] are scaled to be ~ 100 for both for C_1^- in Figure 2. The relative yield for Th^{70+} is three orders of magnitude higher than for Cs^{1+} at the size of C_{16}^- . In both cases the intensity *versus* size dependence can be described by an exponential decay, the decay being much slower for the highly charged ion case. An exponential decay has been ascribed to the applicability of a combinatorial cluster formation model [7, 9, 19]. The reason for the much slower decrease of cluster intensity with cluster size in HCI-induced sputtering of HOPG is presently not understood. Invoking the equilibrium model of Urbassek would ascribe the difference to the amount of energy deposited into the near-surface region. In the HCI case more energy is deposited, bringing the surface closer to, but *not* up to, the critical point. The potential energy of the Th^{70+} is 152.6 keV [20]

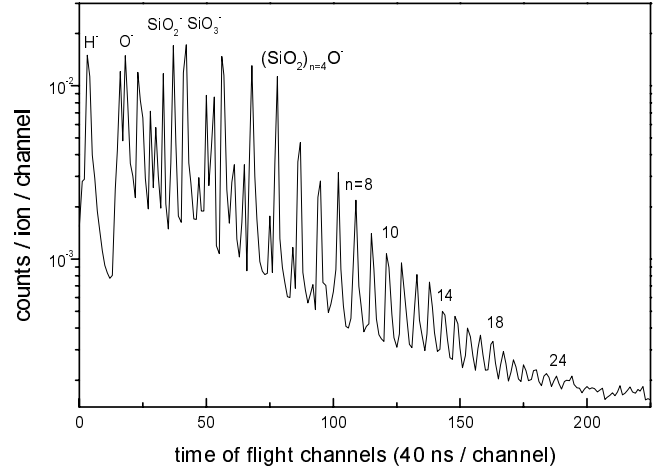


Fig. 3. Negative secondary ion production from SiO_2 (150 nm thermal oxide on silicon) at Th^{70+} impact.

and the kinetic energy loss is approximately 8 keV/nm [13], which corresponds to $\sim 20 \text{ keV/nm}$ over the first 10 nm of the ion-surface interaction. Whereas, the singly charged Cs ion loses $\sim 2 \text{ keV/nm}$ in the first 10 nm of interaction [21].

The question of the presence of a Coulomb explosion-like relaxation of HOPG surfaces at HCI impact and the generation of corresponding shock waves can not be resolved here. Both the shock wave model and the equilibrium model require the deposited energy in the near surface region to remain localized on the time scale of nuclear motion, ~ 100 's of femtoseconds. The potential energy and much of the kinetic energy deposited in the near surface region is initially electronic (or Coulombic) excitation [1, 14]. The transport of electronic excitation in HOPG seems to be high enough to quench some of the near surface excitation before surface atoms or ions can be ejected, and hence the exponential decay of the cluster intensity with size instead of a power law decrease with exponent between -2 and -2.5 (see Sects. 3.2 and 3.3 below).

3.2 SiO_2

Using Th^{70+} ions ($E_{\text{kin}} = 3 \text{ keV/u}$) we also have investigated negative secondary ion production from thin SiO_2 films (Fig. 3). Cluster ions SiO_2^- and $(\text{SiO}_2)_n\text{O}^-$, where n increases from 1 to 24, are observed with intensity decreasing from 2×10^{-2} to 2×10^{-4} cluster ion counts per incident primary ion. Dividing by the detection efficiency gives yields of 20% decreasing to 0.2%. Nanometer sized clusters are produced with high efficiency.

The corresponding cluster yield *versus* size dependence is plotted in Figure 4. For $(\text{SiO}_2)_n\text{O}^-$ clusters, a fit to an exponential decay function ($\sim \exp(-b*n)$) results in a too rapid decrease of the heavy cluster yields. A power law fit ($\sim n^{-a}$) describes the yield decrease *versus* size well in the cluster size range from $n = 3$ to $n = 20$. A least squares

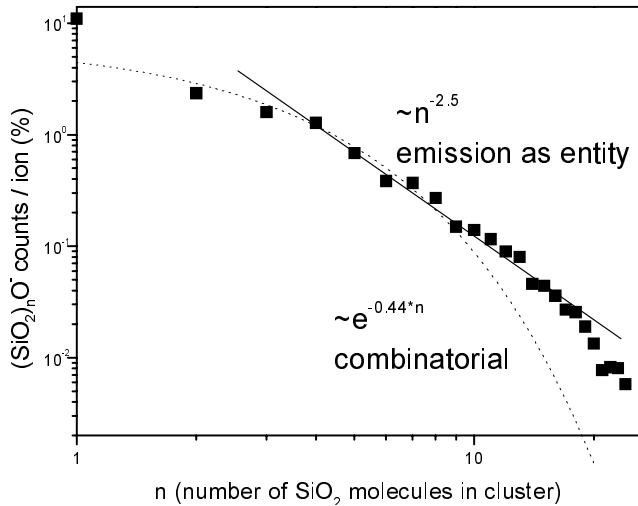


Fig. 4. Negative cluster ion intensities *versus* cluster size, n , for sputtering of thin SiO_2 films by Th^{70+} (3 keV/u).

fit yields a power law exponent of $a = -2.5$. This exponent is much larger than the exponents of $a \in \{-5.5, -9\}$, which were found in singly charged ion-induced cluster emission studies [7], however, the smaller exponents are observed for neutral cluster emission and not ion emission measured here. It is interesting to note that the exponents for both neutral clusters and cluster ions increase as the total sputter yield increases [7], which is not predicted by the models described in the introduction. The near surface excitation caused by the neutralization and impact of Th^{70+} leads both to a high secondary ion yield [1,3], in excess of the total sputter yield for singly charged ions [22,23], and large exponent for the power law dependence of the cluster yield on size.

The exponent of the power law dependence is very close to the predictions of the shock wave model and the equilibrium model. The generation of a shock wave in solids at highly charged ion impact is consistent with the “Coulomb explosion” model, which has been suggested to describe strongly increased secondary ion yields and defect production in the interaction of highly charged ions with surfaces [1,2]. The exponent observed here in the context of the equilibrium model suggests that the energy deposited is sufficient to reach the critical point for the phase transition and that the initial excitation remains localized long enough for nuclear motion to occur (> 100 femtoseconds). The higher relative yield for large clusters from SiO_2 than from HOPG suggests the electronic excitation remains localized longer on the insulating surface than on the semimetal surface.

In recent work, Sporn *et al.* [24] have observed potential sputtering for SiO_2 surfaces for Ar^{q+} ($q < 15$) and Xe^{q+} ($q < 28$). They ascribe the sputtering to the formation of an electronic defect in the surface, “defect mediated sputtering”. The decay of the defect leads to emission of the anion. The loosely bound silicon is then removed by the kinetic energy of the primary ion or a transient volume increase occurring upon defect formation. The cluster

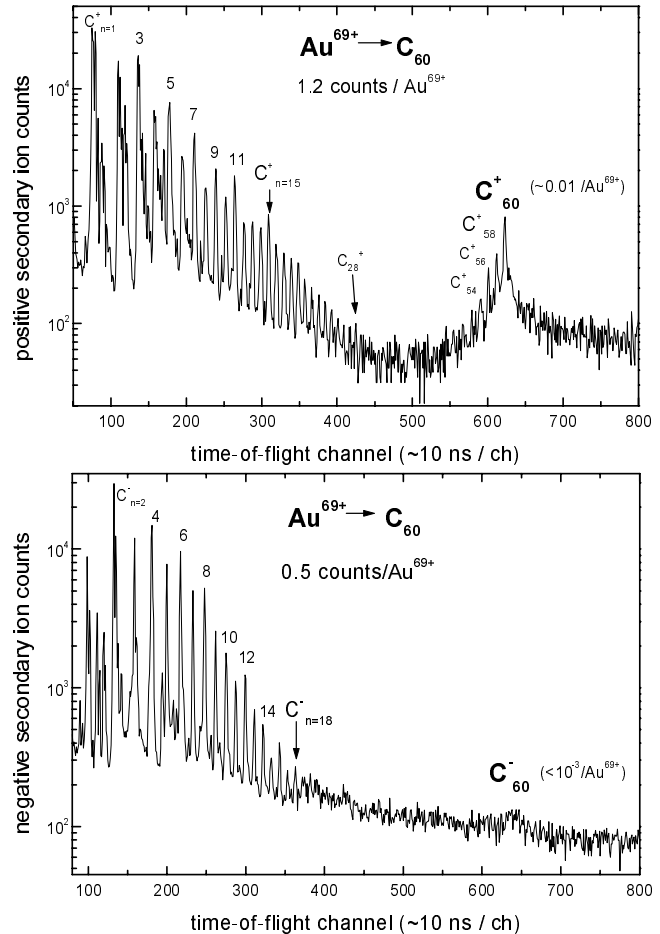


Fig. 5. Positive (a) and negative (b) cluster ion production from a C_{60} surface upon Au^{69+} impact (1.4 keV/u and 3.5 keV/u, respectively).

ion yields observed here favor the volume increase portion of the proposed mechanism. Since a sufficient volume increase may lead to a shock wave, producing efficient cluster emission.

3.3 Fullerenes

Cluster ion yields upon highly charged ion impact are investigated for fullerene surfaces. Figure 5 a and b and Figure 6 shows the positive and negative secondary ion time-of-flight spectra for Au^{69+} impinging on a C_{60} surface and the positive secondary time-of-flight spectrum for Xe^{44+} impinging on a C_{84} surface, respectively. The yield of carbon cluster ions declines with the increase in the size of the C_n cluster for $n = 1$ to $20 < n < 30$. Both odd and even number carbon clusters are observed for $n < 30$. Oscillations are observed in the carbon cluster ion yield as is observed for singly charged and highly charged ion induced cluster ion formation for impact on HOPG (see Sect. 3.1 above). In the positive spectrum, odd-numbered carbon cluster ions are more stable than even-numbered

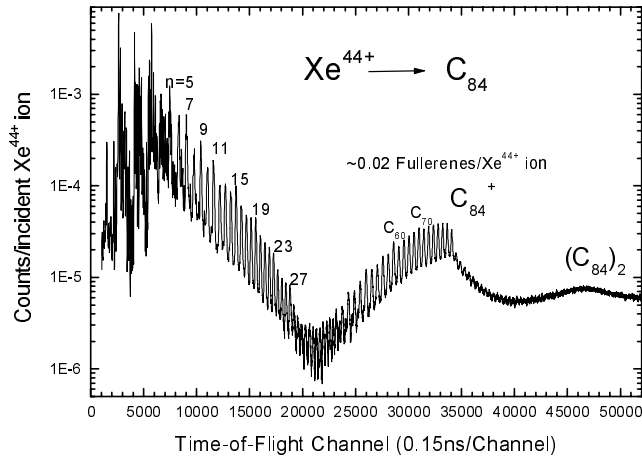


Fig. 6. Positive cluster ion production from a C_{84} surface upon Xe^{44+} impact (1.1 keV/u).

cluster ions up to $n \sim 12$. In the negative cluster ion spectrum, the opposite oscillation is observed. This behavior is ascribed to the electron affinity and ionization potential of linear carbon chains [18]. The oscillation of cluster stability for larger clusters ($n = 15, 19, 23, 27$) can be ascribed to the ion stability of monocyclic ring compounds.

In the positive spectrum for highly charged ion impact of both C_{60} and C_{84} surfaces, large even numbered carbon clusters, but no large odd-numbered clusters, are observed. The most intense signal is observed for the parent fullerene cluster, C_{60}^+ and C_{84}^+ , respectively. For clusters smaller than the parent cluster, the cluster ion yield decreases with decreasing size for $n > 40$. In the C_{84} case, add-on (even-numbered) species are observed as well. The add-on species may be a consequence of the tendency of the fullerenes to polymerize when exposed to light [25] or the closer approach to the critical point (equilibrium model) in the cluster formation process. Interestingly, only very low fullerene cluster yields are seen in the negative cluster ion spectrum, suggesting electron capture during desorption of the C_{60} cluster is an inefficient process in the highly charged ion-induced sputtering. Theoretical studies of fullerene fragmentation suggest that since the carbanion intermediate is involved in the process of negative ion formation and is unstable, the yield of negative fullerene fragment ions will be low [26].

Figure 7 shows the decline in the cluster ion yield *versus* size for Xe^{44+} sputtering of C_{84} for C_n , $n < 30$. The best fit to describe the decline is a power law decrease with an exponent of -2.4 . Both fullerene surfaces have a more gradual decline in the cluster yield with size than the HOPG surface. The higher cluster yields may be ascribed to the less efficient quenching of the highly charged ion-induced surface excitation for fullerene surfaces as compared to HOPG. The fullerenes are semiconducting surfaces with ~ 2 eV bandgaps whereas HOPG is a semimetal with efficient conduction in the basal plane. The highly charged ion-induced cluster yield from a C_{84}

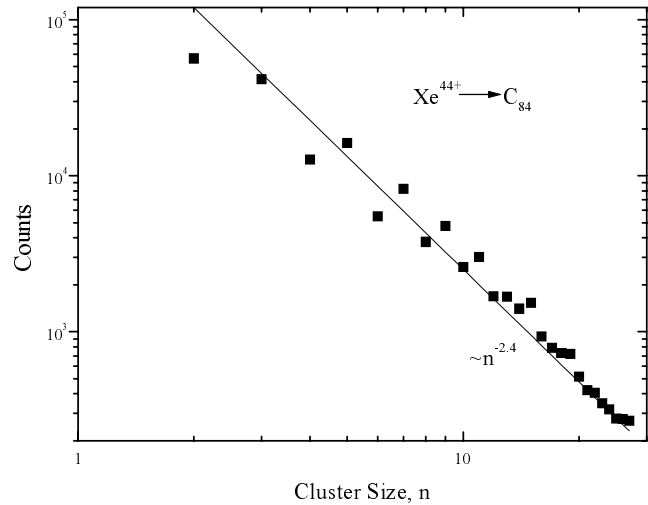


Fig. 7. Positive cluster ion intensities *versus* cluster size, n , for sputtering of C_{84} surface by Xe^{44+} (1.1 keV/u).

surface approaches the -2 exponent limit for the power law.

4 Summary

The emission of large clusters (nanometer-sized) with high efficiency upon sputtering of surfaces with highly charged ions is a phenomenon observed for many materials with a variety of materials properties. The behavior stems from the large potential energy (50 keV for Xe^{44+} to 152 keV for Th^{70+}) that is deposited into a localized near-surface volume upon neutralizing the highly charged ion. The relationship of the cluster yield to the cluster size depends on the lifetime of the localized excitation. The longer the lifetime and the more energy deposited, the closer the power law exponent is to the -2 limit of the equilibrium model and shock wave model. The lifetime seems longer for SiO_2 and fullerene surfaces and shorter for HOPG. The data presented here can not be used to distinguish between the equilibrium and shock wave models.

This work was performed under the auspices of the U.S. Department of Energy at Lawrence Livermore National Laboratory under contract number W-7405-ENG-48.

References

1. D. Schneider, M.A. Briere, *Phys. Scripta* **35**, 228 (1996).
2. M.A. Briere, T. Schenkel, D. Schneider, in *Proceedings of SIMS X*, Münster, October 1995.
3. T. Schenkel, A.V. Barnes, M.A. Briere, A. Hamza, A. Schach von Wittenau, D.H. Schneider, *Nucl. Instrum. Meth. Phys. Res. B* **125**, 153 (1997).

4. A. Wucher, M. Wahl, H. Oechsner, Nucl. Instrum. Meth. Phys. Res. B **83**, 73 (1993).
5. W. Ens, R. Beavis, K.G. Standing, Phys. Rev. Lett. **50**, 27 (1983).
6. W. Begemann, S. Dreihöfer, K.H. Meiwes-Broer, H.O. Lutz, Z. Phys. D **3**, 183 (1986).
7. P. Sigmund, in *Sputtering by Particle Bombardment*, edited by R. Behrisch (Springer, Berlin, Heidelberg, New York, 1982).
8. S.R. Coon, W.F. Calaway, M.J. Pellin, J.M. White, Surf. Sci. **298**, 161 (1993).
9. H.M. Urbassek, Radiation Effects and Defects in Solids **109**, 293 (1989); H.M. Urbassek, Nucl. Instrum. Meth. Phys. Res. B **31**, 541 (1988).
10. R. Gerhard, Z. Physik B **22**, 31 (1975).
11. R.E. Johnson, B.U.R. Sundqvist, A. Hedin, D. Fenyö, Phys. Rev. B **40**, 49 (1989); D. Fenyö, R. E. Johnson, Phys. Rev. B **46**, 5090 (1992).
12. I.S. Bitensky, E.S. Parilis, Nucl. Instrum. Meth. Phys. Res. B **21**, 26 (1987).
13. T. Schenkel, M.A. Briere, A.V. Barnes, A. Hamza, K. Bethge, H. Schmidt-Böcking, D.H. Schneider, Phys. Rev. Lett. **79**, 2030 (1997).
14. T. Schenkel, M.A. Briere, H. Schmidt-Böcking, K. Bethge, D.H. Schneider, Phys. Rev. Lett. **78**, 2481 (1997).
15. D. Schneider, M.W. Clark, B.M. Penetrante, J. McDonald, D. DeWitt, J.N. Bardsley, Phys. Rev. A **44**, 3119 (1991).
16. H. Hong, R.D. Aburano, E.S. Hirschorn, P. Zschack, H. Chen, T.-C. Chiang, Phys. Rev. B **47**, 6450 (1993).
17. H. Hong, W.E. McMahon, P. Zschack, D.S. Lin, R.D. Aburano, H. Chen, T.-C. Chiang, Appl. Phys. Lett. **61**, 3127 (1992).
18. H. Gnaser, H. Oechsner, Nucl. Instrum. Meth. Phys. Res. B **82**, 518 (1993).
19. G. Schiwietz, M. Briere, D. Schneider, J. McDonald, C. Cunningham, Nucl. Instrum. Meth. Phys. Res. B **100**, 47 (1995).
20. R.D. Cowan, in *The Theory of Atomic Structure and Spectra*, (University of California Press) 1981.
21. J.P. Biersack, L.G. Haggmark, Nucl. Instrum. Meth. Phys. Res. **174**, 257 (1980).
22. Y. Yamamura, H. Tawara, At. Data Nucl. Data Tables **62** (1996) p. 149.
23. H. Jacobsson, G. Holmen, J. Appl. Phys. **75**, 8109 (1994).
24. M. Sporn, G. Libiseller, T. Neidhart, M. Schmid, F. Aumayr, HP. Winter, P. Varga, M. Grether, D. Niemann, N. Stolterfolt, Phys. Rev. Lett. **79**, 945 (1997).
25. A.M. Rao, P. Zhou, K.-A. Wang, G.T. Hager, J.M. Holden, Y. Wang, W.T. Lee, X.-X. Bi, P.C. Eklund, D.S. Cornett, M.A. Duncan, I.J. Amster, Science **259**, 955 (1993).
26. R.L. Murry, D.L. Strout, G.E. Scuseria, Int. J. Mass Spectroscopy Ion processes **138**, 113 (1994).